Computationally Efficient Robust Adaptive Beamforming for Passive Sonar

Somasundaram, Samuel; Pilkington, Adrian; Hart, Leslie; Butt, Naveed; Jakobsson, Andreas

2015

COMPUTATIONALLY EFFICIENT ROBUST ADAPTIVE BEAMFORMING FOR PASSIVE SONAR

S. D. Somasundaram[*], *N. R. Butt*[†], *A. Jakobsson*[†], *A. Pilkington*[*], *and L. Hart*[*]

[*]Thales U.K., Maritime Missions Systems, Stockport, U.K.
[†]Dept. of Mathematical Statistics, Lund University, Sweden

ABSTRACT

Recent work has highlighted the benefits of exploiting robust Capon beamformer (RCB) techniques in passive sonar. Unfortunately, the computational requirements for computing the standard RCB weights are cubic in the number of adaptive degrees of freedom, which may be computationally prohibitive in practical situations. Here, we examine recent computationally efficient techniques for computing the RCB weights and evaluate their performances for passive sonar. We also discuss the implementation of these efficient algorithms on parallel architectures, such as graphics processing units (GPUs), illustrating that further significant speed-ups are possible over a central processing unit (CPU) based implementation.

Index Terms— Passive sonar, computationally efficient robust adaptive beamforming.

1. INTRODUCTION

In many passive sonar systems, beamforming is used to form receive beams on hydrophone arrays for the purposes of source localisation, power estimation (acoustic imaging) and for increasing the signal-to-noise ratio (SNR). Conventional delay-and-sum (DAS) beamforming, which applies delays to the hydrophone outputs so that a source signal received in the specified beam direction will appear aligned in the delayed hydrophone outputs, is most often used. Summing the delayed outputs leads to coherent summation of the source signal, but not of noise that is uncorrelated between hydrophone outputs, leading to an increase in SNR. In fact, it is well-known that the DAS beamformer is optimal for a single source in uncorrelated (spatially white) noise [1]. However, in practice, there are typically multiple sources of noise that have significant correlations between hydrophone outputs, including contacts (e.g., shipping) not in the steer direction, platform noise (such as machine induced vibration), flow and flow-induced vibration, ambient noise and biological noise. Shading can be used with DAS beamformers to trade increased mainlobe width (leading to reduced resolution) for lower sidelobe levels, though the desired sidelobe levels are often not met due to imperfect sensor calibration and/or faulty sensors. Alternatively, adaptive beamformers based on Capon or minimum variance distortionless response (MVDR) techniques design data-dependent weights that minimise the array output power subject to a look direction constraint, which, in theory, optimise the array output SNR, even for correlated noise environments. These beamformers are able to adapt their beampatterns to null out correlated noise sources as and when required. The Capon/MVDR weights are a function of the signal-of-interest (SOI) array steering vector (ASV), i.e., the spatial signature due to a SOI in the beam steer direction, and the array covariance matrix. In practice, a model for the SOI ASV, here termed the assumed ASV, and an estimate of the array covariance are used. Unfortunately, errors in these lead to a significant degradation in output SNRs for the standard MVDR/Capon beamformers. SOI ASV errors arise as a result of angle-of-arrival or pointing errors, sensor calibration errors, source wavefront distortions (e.g., due to inhomogeneities in the ocean) and scattering, all of which lead to SOI cancellation. Thus, a wealth of robust adaptive techniques have been proposed to deal with errors in the SOI ASV and covariance matrix estimates (see, e.g., [2, 3] and the references therein). In [4–7], robust Capon beamformer (RCB) techniques [8, 9], exploiting ellipsoidal (including spherical) ASV uncertainty sets, have been shown to systematically allow for mismatch in passive sonar applications, without the need for the ad hoc parameter choices that are often needed with other robust adaptive beamforming methods. Furthermore, they are significantly more robust than Capon/MVDR beamformers to errors in the sample covariance matrix estimate. However, like the Capon/MVDR beamformers, the complexity required to compute the RCB weights is cubic in the number of adaptive degrees of freedom, which can be prohibitive in practice. Further, RCB weight computation requires eigenvalue decomposition (EVD) and Newton search, neither of which are amenable to implementation on parallel hardware such as graphical processing units (GPUs). The purpose of this work is to examine various recent low complexity approximative implementations for computing RCB weights, which require a complexity that is only quadratic in the number of adaptive degrees of freedom and

This work was supported in part by Thales U.K. self-funded research and development, the Swedish Research Council, and Carl Trygger's foundation.

are amenable to implementation, e.g., on GPUs. In [9], it was shown that the RCB weights coincide (within a scale factor) with the worst-case robust adaptive beamformer WC-RAB weights [10, 11] and we will therefore also consider efficient implementations of the WC-RAB. Specifically, we examine the (second-order) constrained Kalman filter implementation of the WC-RAB [12], the gradient-based iterative implementation of the WC-RAB [13], a recursive version of the RCB exploiting variable diagonal loading [14], and a steepest-descent based RCB exploiting scaled projections [15].

2. DATA MODEL, RCB AND WC-RAB

Here, we implement the beamformers in the frequency-domain (see, e.g., [7] for more details) and model the kth frequency-domain snapshot, from frequency bin with centre frequency f, from an M element array as

$$\mathbf{x}_k \triangleq \begin{bmatrix} x_{1,k} & \dots & x_{M,k} \end{bmatrix}^T = \mathbf{a}_0 s_{0,k} + \mathbf{n}_k, \quad (1)$$

where $x_{m,k}$, $\mathbf{a}_0$, $s_{0,k}$, and $\mathbf{n}_k$ denote the kth frequency-domain output of the mth sensor, the SOI ASV, the SOI complex amplitude, and the noise-plus-interference vector, defined similarly to $\mathbf{x}_k$, respectively. Assuming that the noise and interference are uncorrelated with the SOI and that both are zero mean, the array covariance is given by

$$\mathbf{R} \triangleq E\left\{\mathbf{x}_k \mathbf{x}_k^H\right\} = \sigma_0^2 \mathbf{a}_0 \mathbf{a}_0^H + \mathbf{Q}, \quad (2)$$

where $\sigma_0^2 = E\{|s_{0,k}|^2\}$ is the desired signal power and $\mathbf{Q} = E\{\mathbf{n}_k \mathbf{n}_k^H\}$ is the noise-plus-interference covariance. In practice, $\mathbf{R}$ is replaced by the sample covariance matrix (SCM) estimate

$$\hat{\mathbf{R}} = \frac{1}{K} \sum_{k=1}^{K} \mathbf{x}_k \mathbf{x}_k^H. \quad (3)$$

The ASV model for the SOI at frequency f, impinging on the array from location $\boldsymbol{\theta}$, is written as

$$\mathbf{a}(f, \boldsymbol{\theta}) \triangleq \begin{bmatrix} e^{-i2\pi f \tau_1(\boldsymbol{\theta})} & \dots & e^{-i2\pi f \tau_M(\boldsymbol{\theta})} \end{bmatrix}^T, \quad (4)$$

where $\tau_m(\boldsymbol{\theta})$ denotes the propagation delay to the mth sensor, relative to some reference point, for the desired signal impinging from a location described by $\boldsymbol{\theta}$.

2.1. The Robust Capon Beamforming Weights

For a spherical uncertainty set with radius $\sqrt{\epsilon}$, the RCB estimates the SOI ASV by solving [8, 9]

$$\min_{\mathbf{a}} \mathbf{a}^H \mathbf{R}^{-1} \mathbf{a} \quad \text{s.t.} \quad \|\mathbf{a} - \bar{\mathbf{a}}\|_2^2 = \epsilon, \quad (5)$$

where $\bar{\mathbf{a}}$ is the assumed ASV and is usually formed from (4), with $\boldsymbol{\theta}$ set as the beam direction. The Lagrangian function associated with (5) is given by

$$L(\lambda, \mathbf{a}) = \mathbf{a}^H \mathbf{R}^{-1} \mathbf{a} + \lambda \left(\|\mathbf{a} - \bar{\mathbf{a}}\|_2^2 - \epsilon \right), \quad (6)$$

where λ denotes a real-valued Lagrange multiplier. Minimizing (6) with respect to $\mathbf{a}$ yields

$$\frac{\partial L(\lambda, \mathbf{a})}{\partial \mathbf{a}^H} = \mathbf{R}^{-1} \mathbf{a} + \lambda(\mathbf{a} - \bar{\mathbf{a}}), \quad (7)$$

which can be re-arranged to yield

$$\hat{\mathbf{a}} = \left(\frac{\mathbf{R}^{-1}}{\lambda} + \mathbf{I} \right)^{-1} \bar{\mathbf{a}} = \bar{\mathbf{a}} - (\mathbf{I} + \lambda \mathbf{R})^{-1} \bar{\mathbf{a}}. \quad (8)$$

The Lagrange multiplier λ is found from

$$g(\lambda) = \left\| (\mathbf{I} + \lambda \mathbf{R})^{-1} \bar{\mathbf{a}} \right\|_2^2 = \epsilon, \quad (9)$$

which can be solved via the EVD of $\mathbf{R}$ and a Newton search. Substituting the $\hat{\lambda}$ that solves (9) into (8) yields the estimated ASV, $\hat{\mathbf{a}}$. The RCB weight vector is then given by

$$\mathbf{w}_{\text{RCB}} = \frac{\mathbf{R}^{-1} \hat{\mathbf{a}}}{\hat{\mathbf{a}}^H \mathbf{R}^{-1} \hat{\mathbf{a}}}. \quad (10)$$

Using the re-scaled estimated ASV $\hat{\hat{\mathbf{a}}} = \sqrt{M} \hat{\mathbf{a}} / \|\hat{\mathbf{a}}\|_2$ instead of $\hat{\mathbf{a}}$ in (10) leads to more accurate power estimation, but as it amounts to a re-scaling of the weights, it has no effect on the signal-to-interference-plus-noise ratio (SINR). Due to the required EVD, solving the RCB requires $\mathcal{O}(M^3)$ operations.

2.2. The WC Robust Adaptive Beamforming

The worst-case robust adaptive beamformer (WC-RAB) problem, under spherical uncertainty, is formulated as [10]

$$\min_{\mathbf{w}} \mathbf{w}^H \mathbf{R} \mathbf{w} \quad \text{s.t.} \quad \left| \mathbf{w}^H \mathbf{a} \right| \geq 1 \quad \forall \mathbf{a} \in \|\mathbf{a} - \bar{\mathbf{a}}\|_2 \leq \epsilon \quad (11)$$

where the constraints ensure that the distortionless constraint is maintained for the worst-case steering vector contained in the set, i.e., for the steering vector $\mathbf{a}$ such that $\left| \mathbf{w}^H \mathbf{a} \right|$ has the smallest value. The optimization (11), which contains an infinite number of non-convex constraints, can be beneficially re-written using a convex constraint as [10]

$$\min_{\mathbf{w}} \mathbf{w}^H \mathbf{R} \mathbf{w} \text{ s.t. } \mathbf{w}^H \bar{\mathbf{a}} = 1 + \sqrt{\epsilon} \|\mathbf{w}\|_2 \quad (12)$$

providing that

$$\left| \mathbf{w}^H \bar{\mathbf{a}} \right| > \sqrt{\epsilon} \|\mathbf{w}\|_2. \quad (13)$$

The weights that solve (12), here termed the WC-RAB weights, have been shown to be equivalent to the RCB weights in (10) [9]. Thus, in the following sections, we examine efficient approximative implementations of both the RCB and the WC-RAB.

3. KALMAN BASED WC-RAB

The Kalman filter based implementation of the WC-RAB, proposed in [12], starts from the worst-case formulation in (12). The mean square error (MSE) between a desired signal of 0 and the beamformer output is given by

$$\text{MSE} = E\left\{\left|0 - \mathbf{w}^H\mathbf{x}\right|^2\right\} = \mathbf{w}^H\mathbf{R}\mathbf{w}. \tag{14}$$

Therefore, minimizing the MSE in (14) is equivalent to minimizing the beamformer output power, which is the objective function in (12). The constraint function in (12) may be expressed as

$$\left|1 - \mathbf{w}^H\bar{\mathbf{a}}\right|^2 = \left|-\sqrt{\epsilon}\left\|\mathbf{w}\right\|_2\right|^2, \tag{15}$$

or, equivalently,

$$h_2(\mathbf{w}) \triangleq \epsilon\left\|\mathbf{w}\right\|_2^2 - \mathbf{w}^H\bar{\mathbf{a}}\bar{\mathbf{a}}^H\mathbf{w} + \mathbf{w}^H\bar{\mathbf{a}} + \bar{\mathbf{a}}^H\mathbf{w} = 1, \tag{16}$$

allowing the WC-RAB problem (12) to be written as

$$\min_{\mathbf{w}} \text{MSE s.t. } h_2(\mathbf{w}) = 1. \tag{17}$$

Since the Kalman filter is a minimum MSE (MMSE) filter, it can be used to solve (17). We refer the reader to [12] for further details, terming the algorithm the WC-KF beamformer. In this paper, we set the user parameters $\gamma = 1$, $\sigma_s^2 = 0$, $\sigma_1^2 = M^{-2}\bar{\mathbf{a}}^H\hat{\mathbf{R}}\bar{\mathbf{a}}$, and $\sigma_2^2 = 10^{-12}$.

4. GRADIENT MINIMIZATION BASED WC-RAB

We proceed to discuss the gradient minimization based WC-RAB implementation proposed in [13]. It was there noted that the Lagrange function for the WC-RAB problem (12) may be written as

$$J(\mathbf{w},\lambda) = \mathbf{w}^H\mathbf{R}\mathbf{w} - \lambda\Big(\mathbf{w}^H\bar{\mathbf{a}} - 1 - \sqrt{\epsilon}\left\|\mathbf{w}\right\|_2\Big), \tag{18}$$

where λ denotes the Lagrange multiplier. One approach is to set the derivatives of (18) with respect to $\mathbf{w}^H$ and λ to zero and solve for $\mathbf{w}$ and λ; however, this requires an $\mathcal{O}(M^3)$ complexity. Instead, the approach proposed in [13] uses an iterative gradient minimization scheme to update the weight vector as

$$\mathbf{w}_{k+1} = \mathbf{w}_k - \mu_k\boldsymbol{\delta}_k, \tag{19}$$

where, for the kth snapshot, μ_k and $\boldsymbol{\delta}_k$ denote the step-size parameter and the gradient vector of the cost function (18), respectively. Thus, the weight vector is updated in the direction of steepest descent. The gradient is given by

$$\boldsymbol{\delta}_k = \mathbf{R}\mathbf{w}_k - \lambda\left(\bar{\mathbf{a}} - \sqrt{\epsilon}\frac{\mathbf{w}_k}{\left\|\mathbf{w}_k\right\|_2}\right). \tag{20}$$

We refer the reader to [13] for the derivation of the algorithm, which we here term the WC-IG beamformer. After initializing with $\mathbf{R}_0 = \mathbf{I}$, $\mathbf{w}_0 = \bar{\mathbf{a}}$, and $\alpha = 1$, the WC-IG algorithm iterates the steps given in Algorithm 1.

Algorithm 1 The WC-IG algorithm

1: Update the sample covariance matrix $\mathbf{R}_k$.
2: Compute $\mu_k = \alpha\frac{\mathbf{w}_k^H\mathbf{R}_k^2\mathbf{w}_k}{\mathbf{w}_k^H\mathbf{R}_k^3\mathbf{w}_k}$.
3: Update the unconstrained MV weight vector $\hat{\mathbf{w}}_{k+1} = \mathbf{w}_k - \mu_k\mathbf{R}_k\mathbf{w}_k$.
4: **if** $\text{Re}\left\{\hat{\mathbf{w}}_{k+1}^H\bar{\mathbf{a}}\right\} - 1 < \sqrt{\epsilon}\left\|\hat{\mathbf{w}}_{k+1}\right\|_2$ **then**
5: Compute $\lambda = \frac{-b\pm\sqrt{b^2-4ac}}{2a}$, where

$$\begin{aligned} a &= \mu_k^2\Big[\left(\text{Re}\left\{\mathbf{p}_k^H\bar{\mathbf{a}}\right\}\right)^2 - \epsilon\left\|\mathbf{p}_k\right\|_2^2\Big] \\ b &= 2\mu_k\Big[\mathcal{X}\text{Re}\left\{\mathbf{p}_k^H\bar{\mathbf{a}}\right\} - \epsilon\text{Re}\left\{\hat{\mathbf{w}}_{k+1}^H\mathbf{p}_k\right\}\Big] \\ c &= \mathcal{X}^2 - \epsilon\left\|\hat{\mathbf{w}}_{k+1}\right\|_2^2 \end{aligned}$$

with $\mathcal{X} = \text{Re}\left\{\hat{\mathbf{w}}_{k+1}^H\bar{\mathbf{a}}\right\} - 1$ and $\mathbf{p}_k = \bar{\mathbf{a}} - \sqrt{\epsilon}\frac{\mathbf{w}_k}{\left\|\mathbf{w}_k\right\|_2}$. Then, update weights as $\mathbf{w}_{k+1} = \hat{\mathbf{w}}_{k+1} + \mu_k\lambda\mathbf{p}_k$
6: **else**
7: Set $\mathbf{w}_{k+1} = \hat{\mathbf{w}}_{k+1}$.
8: **end if**

5. THE RCB-VDL-SD ALGORITHM

The steepest-descent based RCB with variable diagonal loading (RCB-VDL-SD), introduced in [14], minimises the RCB Lagrange function (6) using gradient minimisation techniques, updating the SOI ASV recursively using

$$\hat{\mathbf{a}}_k = \hat{\mathbf{a}}_{k-1} - \mu_{\text{SD},k}\mathbf{g}_k, \tag{21}$$

where the gradient $\mathbf{g}_k$ is obtained via (7) as

$$\mathbf{g}_k = \mathbf{R}_k^{-1}\hat{\mathbf{a}}_{k-1} + \lambda(\hat{\mathbf{a}}_{k-1} - \bar{\mathbf{a}}), \tag{22}$$

and the optimal step size is given by

$$\mu_{\text{SD},k} = \frac{\alpha_{\text{VDL}}\left\|\mathbf{g}_k\right\|_2^2}{\mathbf{g}_k^H\mathbf{R}_k^{-1}\mathbf{g}_k + \delta}. \tag{23}$$

The inverse covariance matrix $\mathbf{R}_k^{-1}$ is also updated recursively. We refer the reader to [14] for further details, noting that the algorithm is initialized with $\mathbf{R}_0^{-1} = \mathbf{I}$, $\hat{\mathbf{a}}_0 = \bar{\mathbf{a}}$, $\lambda_0 = 0$, $\mathbf{g}_0 = \bar{\mathbf{a}}$, and $\alpha_{\text{VDL}} = 0.01$. The updated SOI ASV $\hat{\mathbf{a}}_k$ and inverse covariance $\mathbf{R}_k^{-1}$ are inserted in the weight equation (10).

6. THE RCB-SP-SD ALGORITHM

In the steepest-descent based scaled projection RCB (RCB-SP-SD), introduced in [15], the RCB Lagrange function (6) is minimised iteratively using gradient minimisation, where the SOI ASV is updated recursively using

$$\tilde{\mathbf{a}}_k = \mathbf{a}_{k-1} - \mu_{\text{SD},k}\tilde{\mathbf{g}}_k, \tag{24}$$

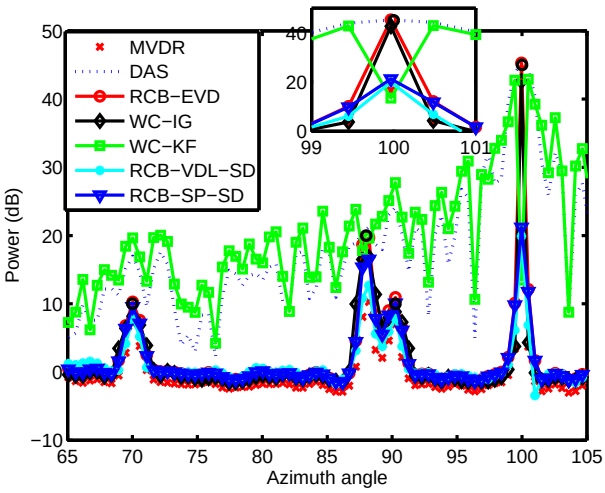

Fig. 1. Spatial spectra for simulated data, assuming $K = 128$.

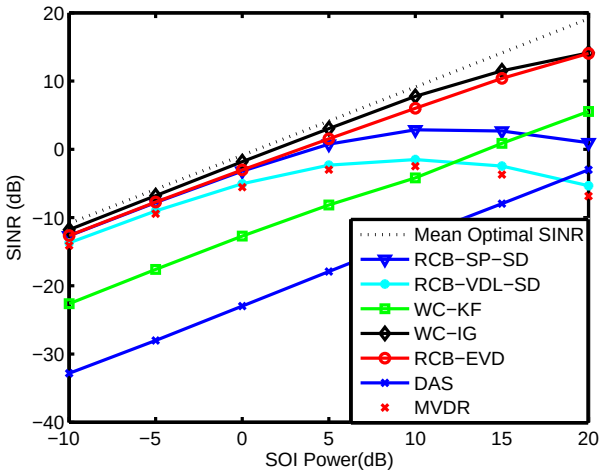

Fig. 2. SINR versus SOI power for $K = 128$.

where

$$\mu_{\text{SD},k} = \frac{1}{\text{tr}\left\{\mathbf{R}_k^{-1}\right\}}, \tag{25}$$

$$\tilde{\mathbf{g}}_k = \mathbf{R}_k^{-1}\mathbf{a}_{k-1}. \tag{26}$$

To satisfy the spherical constraint in (5), $\tilde{\mathbf{a}}_k$ is projected onto the uncertainty set constraint boundary, yielding

$$\mathbf{a}_k = \frac{\sqrt{\epsilon}\,(\tilde{\mathbf{a}}_k - \bar{\mathbf{a}})}{\|\tilde{\mathbf{a}}_k - \bar{\mathbf{a}}\|_2} + \bar{\mathbf{a}}. \tag{27}$$

The updated SOI ASV $\mathbf{a}_k$ and inverse covariance $\mathbf{R}_k^{-1}$ are inserted in the weight equation (10).

7. SIMULATED DATA EXAMPLES

Initially, we evaluate the above discussed algorithms on a simulated half-wavelength spaced uniform linear array with $M = 64$ elements, recreating the simulated scenario described in [6]. The data were simulated using (2) with

$$\mathbf{Q} = \sum_{i=1}^{d} \sigma_i^2 \mathbf{a}_i \mathbf{a}_i^H + \sigma_s^2 \mathbf{I} + \sigma_{\text{iso}}^2 \mathbf{Q}_{\text{iso}}. \tag{28}$$

Thus, the simulated noise plus interference covariance, $\mathbf{Q}$, consists of terms due to d zero-mean uncorrelated interfering sources, where, for the ith interferer, σ_i^2 and $\mathbf{a}_i$ denote the source power and the ASV, respectively, as well as a term modeling the sensor noise $\sigma_s^2\mathbf{I}$, with sensor noise power σ_s^2, and a term modeling an isotropic ambient noise, $\sigma_{\text{iso}}^2\mathbf{Q}_{\text{iso}}$, with power σ_{iso}^2. The isotropic noise covariance is given by

$$[\mathbf{Q}_{\text{iso}}]_{m,n} = \text{sinc}[\pi\lambda(m-n)]. \tag{29}$$

In the following, unless otherwise stated, $d = 3$, $\sigma_s^2 = 0$ dB, $\sigma_{\text{iso}}^2 = 1$ dB, $\sigma_0^2 = 10$ dB, $\sigma_1^2 = 10$ dB, $\sigma_2^2 = 20$ dB, and $\sigma_3^2 = 45$ dB. The AOAs of the discrete interferers are $\theta_1 = 70°$, $\theta_2 = 88°$, and $\theta_3 = 100°$, where the angle of arrival is measured from along the axis of the line array, i.e., from end-fire, so that $\theta \in [0, 180°]$. The azimuth space is sampled using $3M = 192$ equally cosine-spaced beams and the tightest possible spherical uncertainty sets are calculated for each beam, where the sphere centers correspond to theoretical ASVs for the beam centers and the sphere radii were calculated, according to the AOA uncertainty resulting from the spacing of the beams (see, e.g., [4, 5] for further details). The SOI is assumed to belong to the beam whose center is at $\bar{\theta}_0 = 90.25°$. The uncertainty sphere radius (squared) for the SOI beam is $\epsilon = 4.2029$. To allow for the typical case that AOA errors exist, the SOI is simulated anywhere in the interval $[\theta_l, \theta_u]$, where θ_l (θ_u) is the angle midway between the center of the SOI beam and the center of the adjacent beam with lower (higher) angle. Furthermore[1], we assume that the SOI and interference ASVs are subject to independent arbitrary errors and, at each Monte-Carlo simulation, add to each ASV an arbitrary error vector

$$\mathbf{e} = \tilde{\mathbf{e}}/\|\tilde{\mathbf{e}}\|_2, \tag{30}$$

where each element of $\tilde{\mathbf{e}}$ is drawn from a zero-mean circularly symmetric distribution with unit variance. In the following, we examine the beamformer SINR, defined as

$$\text{SINR} = \frac{\sigma_0^2 |\mathbf{w}^H \mathbf{a}_0|^2}{\mathbf{w}^H \mathbf{Q} \mathbf{w}}. \tag{31}$$

It is well known that the optimal SINR is given by

$$\text{SINR}_{\text{opt}} = \sigma_0^2 \mathbf{a}_0^H \mathbf{Q}^{-1} \mathbf{a}_0. \tag{32}$$

[1]We note that our simulated scenario differs slightly to that in [6], as here we have added arbitrary ASV errors to the source ASVs.

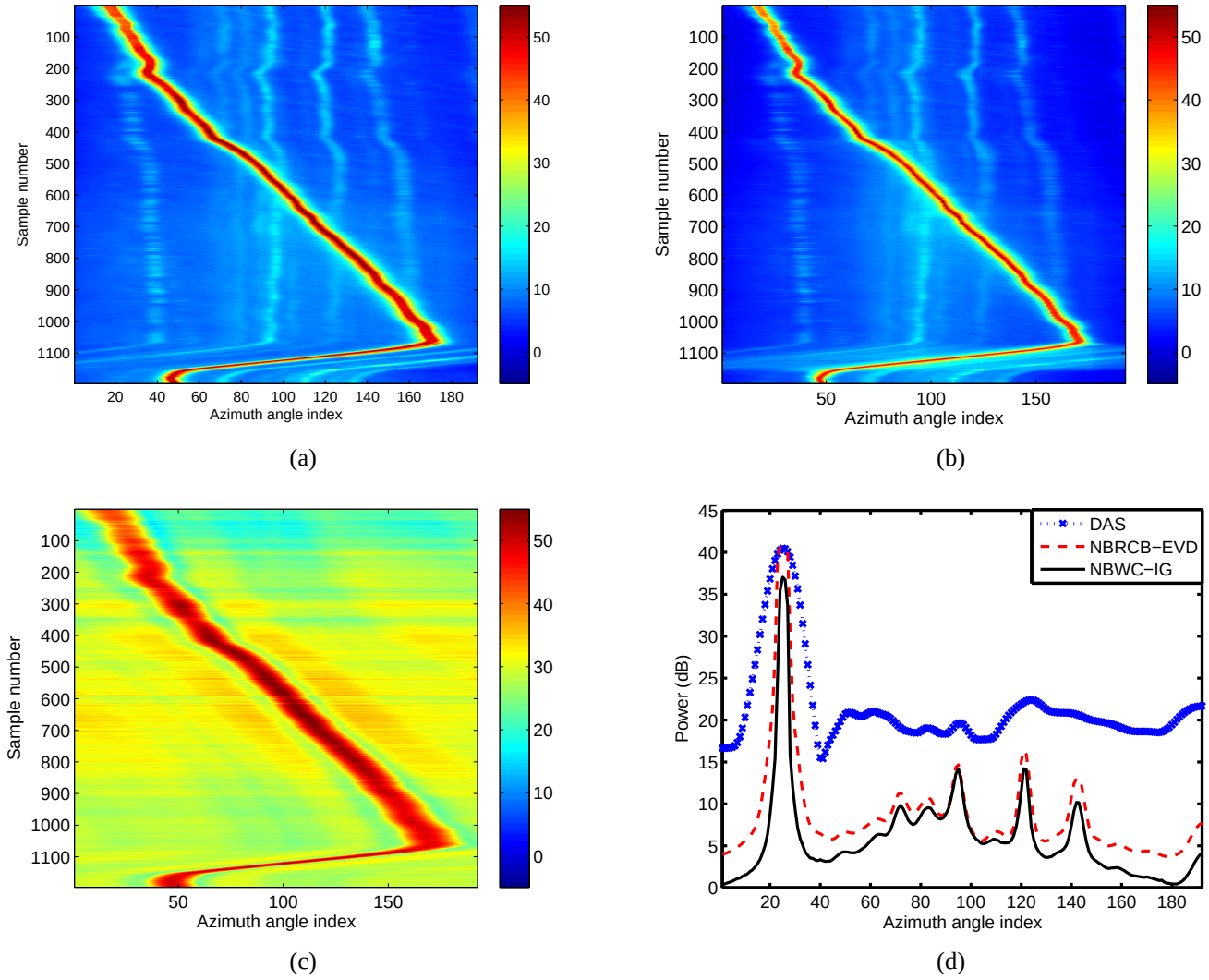

Fig. 3. For the strong controlled source run, bearing time records with $K = 80$ for (a) NBRCB-EVD, (b) NBWC-IG, (c) SDAS. For sample 75, (d) the azimuth spectra.

Since we simulate mismatch in the source ASVs, we compare the beamformer SINRs to the mean optimal SINR, obtained by averaging SINR_{opt} over the Monte-Carlo simulations. We assume that $K = 2M = 128$ snapshots are available for covariance matrix estimation. Figure 1 illustrates the spatial spectra, indicating that MVDR, RCB-SP-SD, and RCB-VDL-SD all exhibit severe SOI cancellation. The standard RCB-EVD provides the best power estimates, followed closely by WC-IG. The Kalman-filter based WC-KF gives poor spatial power estimates. Figure 2 shows the SINR versus the SOI power, clearly showing that WC-IG performs the best out of the efficient techniques and even better than the more complex standard EVD-based RCB. In summary, on simulated data, the WC-IG approach performs the best out of the efficient schemes examined.

8. EXPERIMENTAL DATA RESULTS

We proceed to examine the performance using experimental data from a hull-mounted sonar with $M = 35$ adaptive degrees of freedom, details of which can be found in [7], which contains signals from a known, strong, controlled acoustic source in the far-field of the array, on which we were able to check if the algorithms protected against (desired) signal cancellation, when pointing towards the source, and also their ability to null out the strong source when pointing away from it. We thus proceed to compare results obtained from the RCB-based NBRCB used in [4, 7], which requires EVD and is here denoted NBRCB-EVD, with an implementation based on the WC-IG, which we denote NBWC-IG. In the following, we assume $K = 80$ frequency-domain snapshots per frequency-bin are available for covariance estimation.

Since $K \geq 2M$, we are not here concerned with snapshot deficiency. We also examine results obtained from a shaded DAS (SDAS) beamformer. Figure 3(a)–(c) shows the bearing time records (BTRs), clearly showing that the robust adaptive methods improve the output SNR and spatial resolution compared to the SDAS. Notably, when using robust adaptive beamforming, it is possible to see four weaker sources around beams 40, 90, 125, and 150, which are masked by high sidelobes when using SDAS. Figure 3(d) shows the azimuth spectra for sample 75, which indicates that, for the strong controlled source, the RCB-based NBRCB-EVD power estimates converge to the DAS estimate. Since the strong controlled source power is at least 20 dB greater than any other source or background noise, and is well separated from any other source at sample 75, we expect that its DAS power estimate will be close to the true power [4]. The WC-based NBWC-IG power estimates do not converge to the DAS estimate as a result of the scaling ambiguity that occurs in the worst-case based algorithms.

9. GPU IMPLEMENTATION OF WC-IG

The most computationally intensive step in the standard RCB [8, 9] is the EVD of the covariance matrix, which requires $\mathcal{O}(M^3)$ operations. Further, the EVD is not amenable to implementation on multiple processing units, such as GPUs, as the EVD is not easily parallelisable. As shown by the steps in Algorithm 1, the WC-IG algorithm comprises simple matrix-vector, vector-vector, and scalar operations, which can be performed independently for each beam once the covariance matrix has been updated. Thus, the operations for each beam can be performed on separate processing units, leading to a highly parallelisable implementation. Our C-code version, based on Matlab generated C-code, ran six times slower than real-time on a single core of an Intel Xeon X5670 @ 2.93 GHz, when running 192 frequency bins and 192 beams. Our GPU implementation on an NVIDIA GeForce GTX 580 and coded in CUDA ran more than 20 times faster, confirming that the algorithm is amenable to implementation on GPUs. We remark that in an earlier study we found that the standard RCB ran tens of times slower on GPUs than on a CPU.

10. CONCLUSIONS

In this paper, we have examined four recent efficient (ellipsoid-based) robust adaptive beamforming algorithms. Using simulated data, we conclude that the iterative gradient based implementation of the worst-case robust adaptive beamformer, termed WC-IG, performed the best for the considered passive sonar application. We used the WC-IG approach to implement the recent NBRCB algorithm, terming the efficient implementation NBWC-IG, and evaluated it on recorded passive sonar data in non-snapshot deficient conditions. We found that NBWC-IG performed similarly to NBRCB, and significantly better than the conventional shaded DAS beamformer. In summary, the efficient WC-IG based implementation provide excellent performance at a significantly reduced computationally complexity. We also found that the WC-IG algorithm is amenable to implementation on GPUs and was able to provide significant speed increases over a CPU-based implementation.

11. REFERENCES

[1] P. Stoica and R. L. Moses, *Spectral Analysis of Signals*, Prentice Hall, 2005.

[2] H. L. Van Trees, *Optimum Array Processing: Part IV of Detection, Estimation and Modulation Theory*, Wiley, New York, 2002.

[3] J. Li and P. Stoica, *Robust Adaptive Beamforming*, Wiley, New York, 2005.

[4] S. D. Somasundaram and N. H. Parsons, "Evaluation of Robust Capon Beamforming for Passive Sonar," *IEEE J. Ocean. Eng.*, vol. 36, no. 4, pp. 686–695, Oct. 2011.

[5] S. D. Somasundaram, A. Jakobsson, and N. H. Parsons, "Robust and Automatic Data-Adaptive Beamforming for Multi-Dimensional Arrays," *IEEE Trans. Geosci. Remote Sens.*, vol. 50, no. 11, pp. 4642–4656, Nov. 2012.

[6] S. D. Somasundaram, "Reduced Dimension Robust Capon Beamforming for Large Aperture Passive Sonar Arrays," *IET Radar, Sonar Navig.*, vol. 5, no. 7, pp. 707–715, Aug. 2011.

[7] S. D. Somasundaram, "Wideband Robust Capon Beamforming for Passive Sonar," *IEEE J. Ocean. Eng.*, vol. 38, no. 2, pp. 308–322, Apr. 2013.

[8] P. Stoica, Z. Wang, and J. Li, "Robust Capon Beamforming," *IEEE Sig. Process. Lett.*, vol. 10, no. 6, pp. 172–175, Jun. 2003.

[9] J. Li, P. Stoica, and Z. Wang, "On Robust Capon Beamforming and Diagonal Loading," *IEEE Trans. Signal Process.*, vol. 51, no. 7, pp. 1702–1715, Jul. 2003.

[10] S. A. Vorobyov, A. B. Gershman, and Z.-Q. Luo, "Robust Adaptive Beamforming Using Worst-Case Performance Optimization: A Solution to the Signal Mismatch Problem," *IEEE Trans. Signal Process.*, vol. 51, no. 2, pp. 313–324, Feb. 2003.

[11] R. G. Lorenz and S. P. Boyd, "Robust Minimum Variance Beamforming," *IEEE Trans. Signal Process.*, vol. 53, no. 5, pp. 1684–1696, May 2005.

[12] A. E.-Keyi, T. Kirubarajan, and A. B. Gershman, "Robust Adaptive Beamforming Based on the Kalman Filter," *IEEE Trans. Signal Process.*, vol. 53, no. 8, pp. 3032–3041, Aug. 2005.

[13] A. Elnashar, "Efficient Implementation of Robust Adaptive Beamforming Based on Worst-Case Performance Optimization," *IEEE Trans. Signal Process.*, vol. 2, no. 4, pp. 381–393, Dec. 2008.

[14] A. Elnashar, S. M. Elnoubi, and H. A. El-Mikati, "Further Study on Robust Adaptive Beamforming with Optimum Diagonal Loading," *IEEE Trans. Antennas Propag.*, vol. 54, no. 12, pp. 3647–3658, Dec. 2006.

[15] W. Zhang and S. Wu, "Low-Complexity Online Implementation of a Robust Capon Beamformer," in *Proc. Sensor Signal Processing for Defence*, London, U.K., Sep. 25-27 2012.